ARTICLE OPEN

Check for updates

The effect of metals on zeolite crystallization kinetics with relevance to nuclear waste glass corrosion

Adam J. Mallette[1], Joelle T. Reiser[2], Giannis Mpourmpakis[3], Radha Kishan Motkuri[2], James J. Neeway[2]✉ and Jeffrey D. Rimer[1]✉

Geologic disposal of vitrified radioactive material is planned in several countries, but there are remaining uncertainties related to the long-term stability of glass exposed to groundwater. Specifically, the crystallization of aluminosilicate zeolite minerals can accelerate the rate at which glass corrodes and radioactive material is released into the biosphere. In this study, we identify elemental species that may accelerate or suppress zeolite formation using a protocol to examine their effects on zeolite synthesis over a three-day duration. Our results are consistent with previous works demonstrating glass corrosion acceleration in the presence of calcium. Furthermore, we identify two elements—tin and lithium—as inhibitors of zeolite P2 (gismondine, or GIS type) nucleation and, thus, promising components for promoting the long-term durability of glass waste forms.

npj Materials Degradation (2023)7:4 ; https://doi.org/10.1038/s41529-022-00310-9

INTRODUCTION

Radionuclides from nuclear waste can be incorporated into glass matrices via vitrification to limit their release into the environment after geological disposal. To date, a wide range of proposed or actual borosilicate glass compositions have been developed, which corrode at various rates upon exposure to water. In general, glasses corrode rapidly at first (Stage I) before dissolution rates are reduced to a much slower and (nearly) constant level (Stage II)[1,2]. As the duration of the experiment increases, however, the glass dissolution may increase (Stage III) as a result of several mechanisms[3]. For example, the formation of zeolite crystals[4–8] is correlated with Stage III behavior. Zeolite framework types CHA, ANA, and GIS (three-letter codes refer to crystal structures designated by the International Zeolite Association) have been identified once a glass demonstrates Stage III behavior or are known to induce Stage III behavior when added to the system. Since the ability to modify the durability of waste glasses is effectively limited to their composition, the focus of this study is to understand which oxides in the glass affect (either enhance or inhibit) the formation of zeolitic phases that result in Stage III dissolution behavior.

A vast array of oxides is used in glass formulations, but deconvoluting which elements promote or suppress zeolite nucleation remains challenging. In zeolite synthesis research, various elements in growth mixtures are understood to have distinct and significant effects on crystallization that are briefly surveyed here to summarize reported effects of elements known to alter zeolite formation. Besides Si and Al, which comprise the basic building blocks of natural and most synthetic zeolites, alkali metals are common extra-framework elements in zeolites. Indeed, these ions are often required to achieve fully crystalline products for many framework types because they balance negatively-charged AlO_4^- framework sites[9–15]. Alkali cations also function as structure-directing agents (SDAs) to facilitate the formation of a particular structure[15]. For instance, Kirschhock and coworkers[16] demonstrated that the product of seeded zeolite syntheses can be controlled simply via ion exchange of alkali cations in the parent crystal (Li^+, Na^+, K^+, Rb^+, and Cs^+). Previously, the composition space of zeolites that form in sodium[9] and potassium[4] media has been mapped. Compared to alkali metals, alkaline earth metals (Group II) are rarely used as SDAs in zeolite synthesis; however, these cations are often present in natural zeolites, suggesting their influential role in geologic zeolite formation[17,18]. For instance, calcium[19], magnesium[20], and strontium[21] have each been shown to increase zeolite crystallization rates. Compared to cations, anionic halides (Group VII) have a minor effect on zeolite syntheses[15,22] with one exception: fluoride—which can replace hydroxide as a mineralizing agent (i.e., zeolite accelerant) that facilitates crystal formation with fewer defects[23–29]. The motive for adding elements in the transition metal block and groups III–V to the growth mixture is generally to isomorphically substitute heteroatoms (e.g., Zn, Sn, and Ga) into the crystal structure to enhance catalytic activity. These elements can have diverse effects on zeolite crystallization, which tends to be highly sensitive to the presence of inorganic additives. For example, small amounts of tin (Si/Sn molar ratio = 100) and zinc (Si/Zn molar ratio = 50) can extend the time required to synthesize zeolites BEA[30] and FAU[14], respectively, while germanium can accelerate the synthesis of various framework types[31]. Owing to the complexity of zeolite synthesis mixtures, the underlying mechanistic causes of these phenomena are typically challenging to deconvolute.

To elucidate the effects of certain elemental oxides on glass corrosion, Crum et al.[32] designed a matrix of 24 waste glasses (Supplementary Table 1) called the enhanced low-activity waste (eLAW) matrix. In particular, the matrix was subjected to a series of tests where zeolite P2 (GIS type, or gismondine) seeds were added to the glass-water system at pre-determined durations to help understand the propensity for various glass compositions to exhibit induced Stage III behavior. The statistically designed matrix was developed for compositions pertinent to the Hanford Waste Treatment and Immobilization Plant (WTP)[33]. Seven major components (Al_2O_3, B_2O_3, CaO, Na_2O, SiO_2, SnO_2, and ZrO_2) were varied independently, while all remaining species were grouped into an eighth component (listed generically as "*others*"), which was also varied. The matrix was designed such that the individual

[1]Department of Chemical and Biomolecular Engineering, University of Houston, Houston, TX 77204, USA. [2]Pacific Northwest National Laboratory, Energy and Environment Directorate, Richland, WA 99354, USA. [3]Department of Chemical and Petroleum Engineering, University of Pittsburgh, Pittsburgh, PA 15213, USA.
✉email: james.neeway@pnnl.gov; jrimer@central.uh.edu

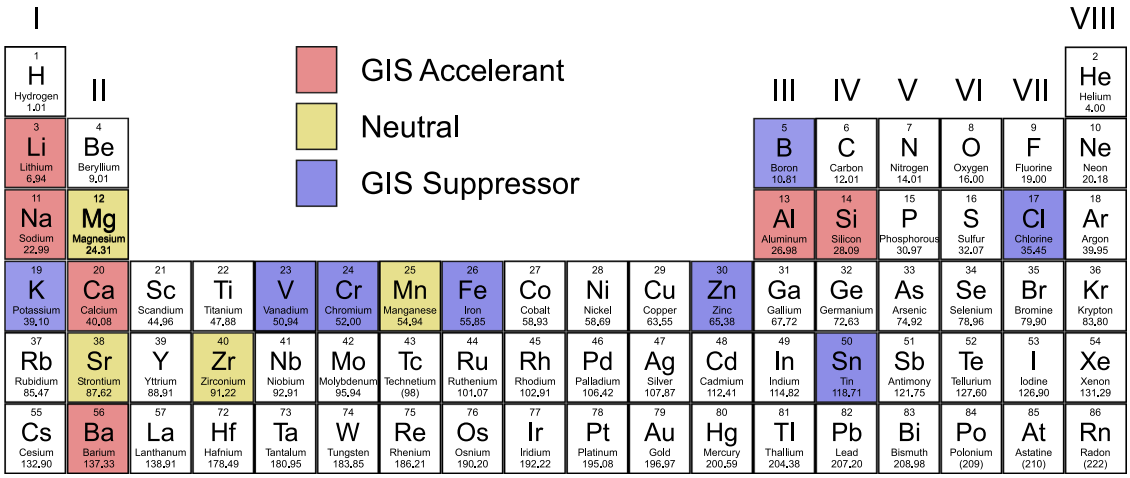

Fig. 1 Periodic table. Effect of elemental species on zeolite GIS crystallization rates using conventional synthesis conditions. Each synthesis was carried out for 3 days at 100 °C using a growth mixture with a molar composition of 9 SiO_2:0.5 Al_2O_3:5.5 Na_2O:0.2 M_xO_y:190 H_2O. Growth mixtures have a pH value of ~13. Reagent "M" corresponds to the element added (see the "Materials" section for details), which is color-coded according to its effect on the crystallization rate: accelerant (red), suppressor (blue), or neutral (yellow).

effects of the seven major components and *others* could be isolated. In the study by Crum et al.[32], each of the 24 glasses was allowed to react with deionized water at 90 °C in a stainless steel vessel for 28 days. Then, seeds of zeolite P2 (GIS type) were added to the system and the experiment continued at 90 °C to observe whether or not the presence of the zeolite seeds affected the glass dissolution rate over the following twelve months. The addition of zeolite seeds has the potential to induce Stage III glass behavior on reasonable time scales[8], and zeolite P2 is used because it is one of the most common zeolites known to induce Stage III glass behavior[34]. Zeolite P2 is one of two common polymorphs possessing the GIS framework; the other is P1 (Supplementary Fig. 1a), which is differentiated by a slight twist in the channel geometry that has been described in detail elsewhere[14,35]. Crum et al.[32] distinguished four types of glass behaviors depending on their composition: (Type 1) no effect of the seed, (Type 2) an immediate increase in the glass dissolution rate until all of the glass dissolved, (Type 3) an immediate increase in the glass dissolution followed by an eventual slowing in the rate, and (Type 4) an increase in the glass dissolution rate that was offset with respect to the time that the seeds were added. Most significantly, glasses with low calcium content resisted Stage III behavior significantly better than those with relatively high calcium content.

Though previous observations have been helpful in identifying the glass compositions that may be susceptible to Stage III dissolution behavior, the role of zeolite crystallization kinetics is still unclear because zeolite seeds were added to the system, thus bypassing nucleation. Herein, we attempt to isolate the role of crystallization kinetics by simulating the glass composition stoichiometrically (except for NaOH, which was added in excess to attain a high solution pH) and identifying the resulting zeolite-containing product. This method allows us to bypass certain experimental constraints (i.e., long analysis times) in the glass dissolution tests and isolate the role of select zeolite accelerants and suppressors. In this study, we discuss the consequences of various elements on zeolite crystallization kinetics in conventional synthesis mixtures. Selecting elements present in waste glass at high compositions, we perform systematic studies using zeolite synthesis mixtures that more accurately simulate the composition of borosilicate glasses. We show that modifications to zeolite growth mixtures by alkali metal substitution and/or alkaline earth metal addition can significantly alter crystallization rates. This approach aids the identification of certain glass compositions that may be susceptible to Stage III behavior in the environment and allow nuclear disposal facilities to potentially mitigate the occurrence of Stage III behavior due to zeolite crystallization.

RESULTS AND DISCUSSION

Elemental effects in conventional zeolite synthesis media

The effects of many elements present in the eLAW glass compositional matrix were investigated by adding each to a conventional synthesis[35] of zeolite P2 (GIS), one of the most common frameworks observed as an accelerant of nuclear waste glass dissolution rates (Supplementary Fig. 1a)[36]. Synthesis mixtures have a molar composition of 9 SiO_2:0.5 Al_2O_3:5.5 Na_2O:0.2 M_xO_y:190 H_2O (where M = metal, x = number of M atoms, and y = number of O atoms) and were treated for 3 days at 100 °C, which is sufficient for complete crystallization of GIS, by way of a FAU intermediate pathway, in a conventional zeolite synthesis (i.e., M = 0, Supplementary Fig. 2). Additional details are discussed in the Methods section below. The hydrothermal treatment temperature was selected to be consistent with well-characterized zeolite syntheses.[9,35] Analysis of product powder X-ray diffraction (PXRD) patterns reveals that many higher valence elements (e.g., Cr, B, Zn, Sn, Fe) suppress GIS formation (Fig. 1, blue and Supplementary Fig. 3a). Most notably, tin and zinc completely inhibit GIS crystallization for longer than 28 days of heating. The observation of a small FAU impurity in PXRD patterns was used to distinguish elements that do not appear to alter crystallization rates (Mg, Sr, Zr, and Mn, Fig. 1, yellow; and Supplementary Fig. 3b) from those that accelerate the formation of zeolite products (notably, Na, Li, and Ca; Fig. 1, red; and Supplementary Fig. 3c), where FAU is absent from PXRD patterns of GIS crystals[35].

Elemental effects in simulated glass synthesis media

Following the initial survey of elements under conditions that are typical of synthetic zeolites, we sought to explore the effect of elements when synthesis mixtures more accurately reflect the complex environment of altered nuclear waste glass. Our assumption is that all glass components are released congruently from the glass into solution whereas it is well known that the release of species from the glass is incongruent in static dissolution tests. In addition, the present set of experiments ignores the possible effect that an altered glass substrate may play in zeolite nucleation kinetics. For a basis, we selected the seven major components (Al, B, Ca, Na, Si, Sn, and Zr) present in the eLAW series of 24 glasses assayed by Crum et al.[32] In the study carried out by

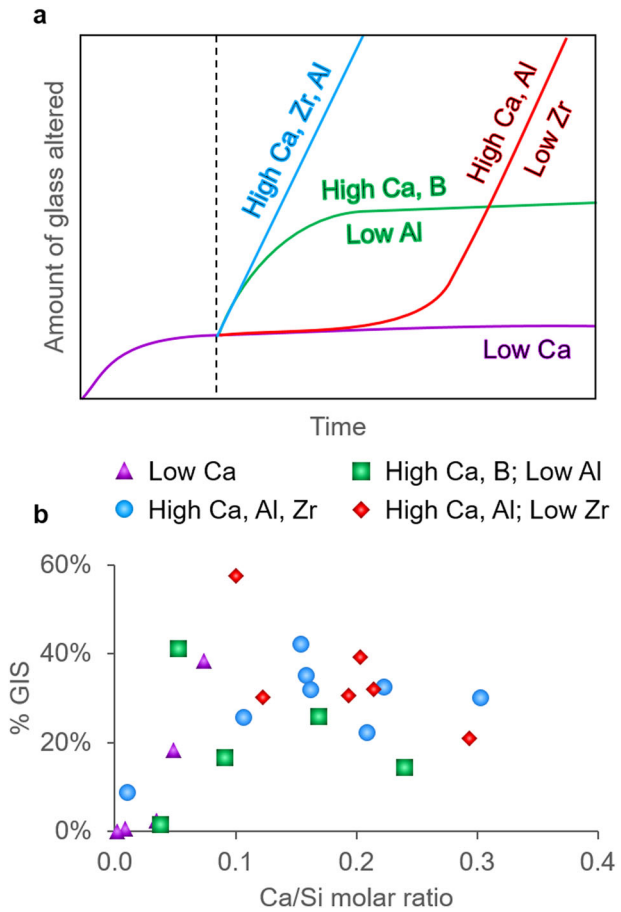

Fig. 2 Effect of Ca. a Qualitative response curves of eLAW glasses in dissolution studies performed in the presence of zeolite seeds, as reported by Crum et al.[32]. Seed addition (dashed vertical line) allows for glass responses to be assayed on a reasonable timeframe. Glasses are characterized and grouped according to their compositions: Type 1, low CaO (purple); Type 2, high CaO, Al_2O_3, ZrO_2 (blue); Type 3, high CaO, B_2O_3, and low Al_2O_3 (green); and Type 4, high CaO, Al_2O_3, and low ZrO_2 (red). **b** Experimentally observed weight fraction of zeolite GIS phase in the product of bulk crystallization versus Ca/Si molar ratio in the initial synthesis mixtures designed to mimic eLAW glass conditions. Exact molar compositions and product phase information are presented in Supplementary Tables 2 and 5, respectively. Color coding of data points is based on the classification of each glass according to panel **a**, which corresponds to alteration responses for glasses with low CaO (purple triangles); high CaO, Al_2O_3, ZrO_2 (blue circles); high CaO, B_2O_3, and low Al_2O_3 (green squares); and high CaO, Al_2O_3, and low ZrO_2 (red diamonds). Elemental forms rather than oxide forms are used in the figure for brevity. Panel **a** is recreated with permission adapted with permission from ref. [32], Copyright 2021 by John Wiley and Sons.

Crum et al.[32], observations after seeding (Fig. 2a) could be described with four different behavior types (and general compositional trends): (Type 1) no effect of the seed (low CaO), (Type 2) an immediate increase in the glass dissolution rate until all of the glass dissolved (high CaO, Al_2O_3, and ZrO_2), (Type 3) an immediate increase in the glass dissolution followed by an eventual slowing in the rate (high CaO, B_2O_3, low Al_2O_3), and (Type 4) an increase in the glass dissolution rate that was offset with respect to the time that the seeds were added (high CaO, Al_2O_3, low ZrO_2). These glass classification types were made based on the general composition properties of groups of glasses that exhibited similar responses in glass dissolution experiments. For instance, not every Type 4 glass necessarily has a high CaO content. For the zeolite syntheses in this study, the appropriate molar ratios were calculated where several values (H_2O, OH, and Si based on the previous studies[9,15]) were held constant to maintain consistency across synthesis mixtures (Supplementary Tables 3 and 4). To assess the effects of changing molar ratios, we heated each of the 24 mixtures, labeled eLAW-*X* ($X = 1$–24, Supplementary Table 2), for 7 days at 100 °C. In most cases, we observed a mixture of amorphous and crystalline (both zeolitic and non-zeolitic) phases in the products. Quantitative analysis of crystalline phase(s) was performed by refining (PXRD patterns with the software Topas (Supplementary Fig. 4) using MgO as an internal standard. In most cases, the dominant zeolite phase is GIS, but in select cases we observed crystals of metastable zeolite frameworks FAU (Supplementary Fig. 1b) and LTA (Supplementary Fig. 1c) that often form at similar synthesis conditions[9,37–41]. Among non-zeolitic phases, the most prominent is burtite, or calcium hexahydroxystannate ($Ca[Sn(OH)_6]$), which varies in weight fraction across the samples where it was detected (Supplementary Table 5). Another precipitated non-zeolitic phase includes zirconium oxide (ZrO_2), but it did not appear to influence zeolite crystallization in these experiments since its composition in the product could not be correlated to the fraction of GIS product (Supplementary Figs. 4–6).

The phase outcomes of 24 eLAW zeolite syntheses from this study produced several noteworthy correlations to the behaviors presented in Fig. 2a. First, these findings revealed that short (<7 days) and facile experiments may be capable of quickly assessing the susceptibility of certain glass compositions to precipitate zeolites much more rapidly than glass dissolution tests, which are both time- and resource-intensive. Among the seven components investigated, we identified two (calcium and tin) that most significantly impact zeolite crystallization; the fraction of zeolite GIS is not directly correlated with any other element (Supplementary Fig. 6). These observations corroborate the results reported by Crum et al.[32] which suggest higher calcium content promotes zeolite formation and Stage III behavior (Fig. 2a). Indeed, a significant increase in the fraction of zeolite GIS product is apparent as the amount of calcium in the growth mixture increases (Fig. 2b and Supplementary Fig. 7). Synthesis mixtures with the lowest amount of calcium (Ca/Si < 0.1) led to largely amorphous products and/or metastable zeolite phases, which suggests that a longer time is required for GIS crystallization. Increasing the amount of calcium to intermediate levels ($0.1 < Ca/Si < 0.2$) led to a significant increase in the amount of zeolite GIS formed. High calcium content (Ca/Si > 0.2) can slightly decrease the relative amount of zeolite GIS, which may be related to the tendency of Ca^{2+} ions to precipitate as $Ca(OH)_2$ in alkaline solutions, thus decreasing growth mixture pH. This effect is particularly evident in the case of glasses with high Ca and Al content and low Zr content (Fig. 2a, red diamonds; see also Supplementary Fig. 7). Our finding that calcium promotes the nucleation of zeolite GIS aligns with computational investigations by Mpourmpakis and coworkers[42], who demonstrated that calcium cations substantively enhance the thermodynamic favorability of (alumino)silicate oligomerization.

The precise effect of tin on these systems is more challenging to discern compared to calcium given that several experimental observations are in apparent contradiction. First, our findings reveal that there is no clear correlation between the initial tin composition and the fraction of zeolite GIS product (Supplementary Fig. 6). The quantity of tin is, however, correlated with the amount of burtite in the solid product (Fig. 3a), which is not observed for other elements (Supplementary Fig. 8). Burtite is a crystalline structure that contains calcium (Fig. 3b); therefore, we hypothesize that tin plays a minor role in the suppression of GIS by sequestering calcium in the form of a solid mineral where it cannot promote zeolite nucleation. To this end, we demonstrated that burtite crystallizes prior to zeolite phases (Fig. 3c), which agrees with previous findings[43] and supports our hypothesis that burtite formation reduces the amount of calcium available for

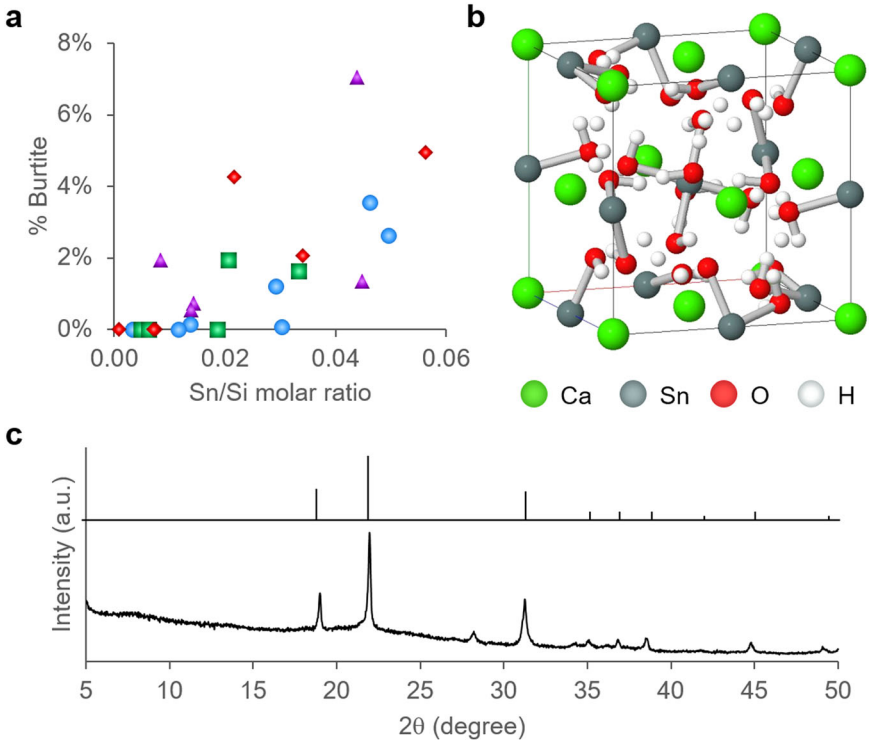

Fig. 3 Effect of Sn. a Graphical relationship illustrating the positive correlation between the weight fraction of burtite in products of eLAW zeolite synthesis series and the amount of tin in the growth mixture. Refer to the legend in Fig. 2b for symbol descriptions. **b** Burtite crystal structure, obtained from the Hudson Institute of Mineralogy using dat from ref. [43]. **c** PXRD pattern of burtite (bottom) synthesized by aging zeolite growth mixture eLAW-24, which had the highest Sn/Si molar ratio (Supplementary Table 2), for 24 h at room temperature without hydrothermal treatment. Reference pattern for burtite (top) was obtained from the American Mineralogist Crystal Structure Database.

promoting zeolite nucleation. In a standard static glass corrosion experiment, this phase may not be observed; however, tin may play a role in preventing the release of calcium into solution by forming less soluble burtite crystals.

It is well-known that zeolite crystallization is commonly suppressed by the presence of tin[30,44–46] even in the absence of calcium, which we have confirmed using a conventional zeolite synthesis mixture (Fig. 1). In this analysis, we aimed to deconvolute the effects of tin and calcium by comparing the result of a synthesis with tin and without calcium to a case where both calcium and tin were absent. We selected eLAW-21 for this study because it led to a large amount of GIS product (Supplementary Fig. 4). For the control synthesis using tin- and calcium-free media, we observed the formation of a zeolite product predominantly comprised of GME (Fig. 4, pattern *i*), which has a structure (Supplementary Fig. 1d) similar to that of GIS (Supplementary Fig. 1a). When another synthesis was carried out in the presence of tin, we instead observed a largely amorphous product (Fig. 4, pattern *ii*) with a minor zeolite LTA phase. Therefore, tin clearly suppresses zeolite crystallization in syntheses replicating glass compositions irrespective of calcium content. Notably, tin seemingly affects the propensity of zeolite nucleation to occur in glass solution systems wherein we posit two potential mechanisms for its mode of action: (i) tin sequesters calcium accelerants and/or (ii) stannosilicate oligomers scavenge silica to form species that are putatively less amenable to zeolite nucleation compared to aluminosilicates[46]. The fraction of GIS product is more directly correlated with the concentration of calcium than that of tin (Fig. 2b and Supplementary Fig. 6). This is partly attributed to the relatively high Ca/Si ratio in zeolite growth mixtures but is more likely because tin favors burtite crystallization over that of GIS, as reflected in the changing product distribution as a function of Sn/Ca ratio (Fig. 5).

Throughout this work, the P1 polymorph of zeolite GIS was observed. The prevalence of zeolite P1 in the present study can be due to the limited quantity of available Si species as prior research[35] has established that zeolite P1 preferentially nucleates rather than zeolite P2 at low Si/OH ratios. Owing to the highly viscous synthesis mixture and diversity of sol-gel species, most of the Si species present may be bound in colloidal forms that are not available for zeolite nucleation, lowering the effective Si/OH ratio. Since previous glass dissolution studies showed similar responses regardless of whether zeolites P1 or P2 seeds were added to the system[34,47], the observed trends from this study would likely not substantively change if zeolite P2 were to nucleate from the same growth solutions rather than zeolite P1.

Alkali metal effects in simulated glass synthesis media

Sodium is the most common alkali metal used to promote zeolite synthesis, so its prevalence in many nuclear waste glass compositions suggests that the partial substitution of sodium with alternative alkali metals may enhance glass stability with respect to Stage III behavior. We used eLAW-21 (Supplementary Table 2) as the basis for these syntheses since it leads to a product with a relatively high fraction of zeolite GIS. Increasing the sodium content in the growth mixture to 120% of its original value leads to minimal changes, as expected (Fig. 6, pattern *i*). When potassium is added to the synthesis mixture (Na/K = 5), a partial zeolite MER phase is observed in the product (Supplementary Fig. 1e; and Fig. 6, pattern *ii*), which is consistent with conventional zeolite syntheses where K^+ directs MER formation under otherwise similar conditions as GIS. Given that Li^+ is known to promote zeolite ABW[16], its addition was expected to lead to a dual mixture of GIS and ABW. Contrary to expectations, adding lithium to the synthesis mixture (Na/Li = 5) led to a largely amorphous product with a relatively small quantity of zeolite GIS product

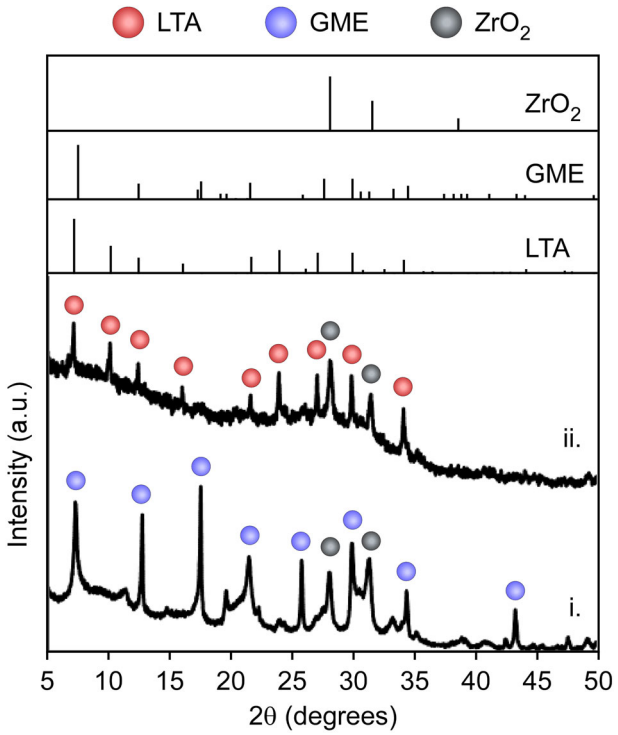

Fig. 4 Deconvoluting Sn and Ca. PXRD patterns illustrating the effect of tin on samples synthesized with a molar composition similar to that of eLAW-21 (Supplementary Table 2). (i) eLAW-21 synthesis repeated in the absence of Ca and Sn. (ii) eLAW-21 synthesis repeated in the absence of Ca and in the presence of Sn. Solid products were extracted from syntheses after 7 days at 100 °C. Reference patterns of ZrO_2, GME, and LTA are provided. The PXRD pattern of solid generated from the original eLAW-21 synthesis is displayed in Supplementary Fig. 4 for reference.

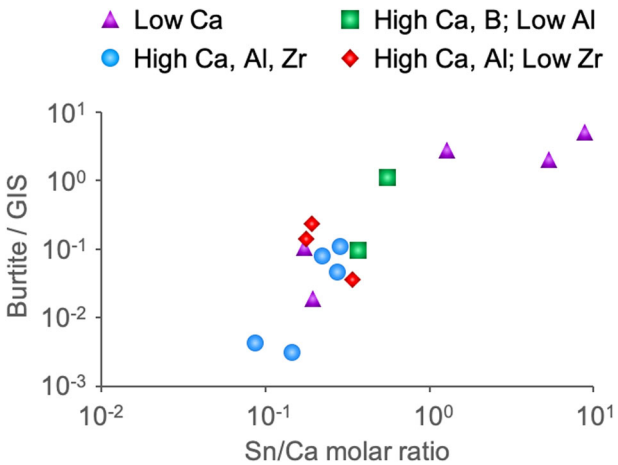

Fig. 5 Effect of Sn/Ca ratio. Logarithmic relationship between the relative amounts of burtite and GIS by weight in the final product (calculated from PXRD patterns using MgO as an internal standard) as a function of the initial Sn/Ca molar ratio of the growth mixture. Color coding of data points is based on the classification of each glass according to Fig. 2a, which corresponds to alteration responses for glasses with low CaO (purple triangles); high CaO, Al_2O_3, ZrO_2 (blue circles); high CaO, B_2O_3, and low Al_2O_3 (green squares); and high CaO, Al_2O_3, and low ZrO_2 (red diamonds). Some samples are not plotted, which do not contain a quantifiable amount of burtite according to their PXRD pattern. Elemental forms rather than oxide forms are used in the figure for brevity.

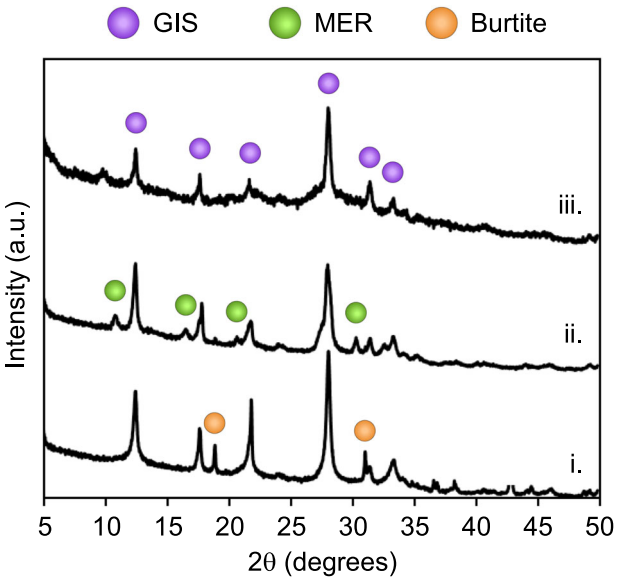

Fig. 6 Alkali metal substitution. Normalized PXRD patterns of products generated from a synthesis mixture designed to simulate the glass composition of eLAW-21 (Supplementary Table 2) with variations in the alkali metal content. Growth mixtures were prepared with molar compositions of 60.5 SiO_2:8.7 Al_2O_3:29.8 Na_2O:6 M_2O:11.2 B_2O_3:2.0 ZrO_2:6.1 CaO: 2.1 SnO_2:1270 H_2O where M = Na (i), K (ii), and Li (iii). All syntheses were carried out for 7 days at 100 °C. Synthesis (i) contains 120% the amount of sodium present in eLAW-21. PXRD patterns are normalized for clarity.

(Fig. 6, pattern *iii*), as indicated by the higher background intensity of the normalized pattern. This result is particularly surprising since the addition of lithium to a similar synthesis using conventional conditions (i.e., in the absence of the extra components used to mimic the glass composition) accelerates GIS crystallization (Supplementary Fig. 9). This suggests that lithium may be altering the physicochemical structure of amorphous precursors or the nature of calcium species in such a way that significantly inhibits zeolite nucleation. Collectively, this result illustrates the importance of using synthesis mixtures that effectively isolate the impacts of individual elements. Furthermore, simple modifications to glass (or synthesis mixture) compositions can significantly reduce the likelihood of zeolite nucleation, with the potential to dramatically enhance the durability of waste glass.

To conclude, studies of zeolite synthesis where crystals nucleate from a mixture designed to simulate glass compositions are a valuable and efficient tool in assessing the likelihood that zeolites will precipitate during nuclear waste glass disposal. Results presented herein correlate well with expectations based on prior dissolution studies,[32] where borosilicate glasses with low calcium content were the least likely to have increased dissolution rates when zeolite seeds were added, even if the synthesis mixtures have a higher pH (~13) than typical glass corrosion experiments (~pH 10). Chemical insights from this study can provide a basis for future work towards predicting nuclear waste glass stability in a disposal scenario. We identify calcium as a promotor of zeolite GIS crystallization and both tin and lithium as inhibitors. Additional promotors and inhibitors have also been identified in conventional zeolite synthesis mixtures, but the correlation between these syntheses and the effects of glass composition on initiating Stage III behavior is less clear (Supplementary Fig. 9), especially in light of the retention of certain species in the alteration layer during glass corrosion. Namely, it has been shown that waste glasses do not dissolve homogeneously[48]. This is an aspect not fully captured in our model system, which overlooks some physical properties of the glass dissolution environment by

assessing a colloidal gel rather than a solution and pristine glass separated from the bulk solution by an alteration layer. Another factor that is overlooked in this study is the impact of zeolite framework type on glass dissolution. Zeolite crystallization functions as a "sink" for removing Si and Al species from glass; therefore, we posit its impact on Stage III behavior is proportional to the rate of zeolite crystallization. We also do not consider the potential impact of radiation in glass corrosion[49]. Indeed, it has been demonstrated that radiation can accelerate the formation of zeolite crystals via hydroxyl radicals[50]. Further investigations into these topics would be beneficial but are outside the scope of this study. This information can be used as a guide to design nuclear waste glass compositions that may be less susceptible to Stage III behavior.

Insights from this study also benefit the zeolite synthesis community. The systematic way this study was conducted provides a strategy for investigating the effects of diverse species on zeolite syntheses. Perhaps one of the more surprising aspects of these results is that some elements (i.e., Ca and Sn) have a dramatic effect on crystallization outcomes while others (i.e., Zr and B) do not appear to have a substantial effect. However, the findings for this system may not be generalizable to syntheses of other zeolite topologies. Future investigation will be necessary to broaden the scope of this research to develop a more holistic understanding of how heteroatoms and other additives alter crystallization mechanisms across the ever-expanding library of zeolite framework types.

METHODS

Materials

The following reagents were used for zeolite synthesis as purchased without further purification: LUDOX AS-40 colloidal silica (40 wt% suspension in water), sodium aluminate (anhydrous), sodium hydroxide (98% pellets), sodium chloride (99.5%), lithium hydroxide (anhydrous, 98%), potassium hydroxide (>85%), tin (IV) chloride pentahydrate, zirconium (IV) oxide, ammonium metavanadate, chromium chloride hexahydrate, manganese (II) nitrate tetrahydrate (97%), iron (III) chloride hexahydrate, zinc nitrate hydrate (98%), boric acid (99.5%), copper nitrate hydrate, magnesium hydroxide (95%), magnesium oxide (99.4%), calcium hydroxide (95%), strontium hydroxide octahydrate (95%), barium hydroxide octahydrate (95%), and zinc oxide (99.9%). Deionized (DI) water was produced with an Aqua Solutions purification system.

Conventional zeolite synthesis

Growth mixtures were prepared with molar compositions 9 Si:1 Al:0.5 M:11 NaOH:190 H_2O where M represents Li, Na, K, Mg, Ca, Sr, Ba, Zr, V, Cr, Mn, Fe, Zn, Sn, Cl, or B. Growth solutions were prepared in a polypropylene (PP) bottle. First, sodium hydroxide and sodium aluminate were dissolved in DI water under 5 min of magnetic stirring. Next, the M containing reagent was added (except for the control, where M = 0) and stirred either for 10 min or until dissolved. Then, LUDOX AS-40 was added using a plastic pipette, whereupon the synthesis mixture coagulated. The gel was immediately shaken, then stirred for 24 h at room temperature using a magnetic stir bar. After this, the synthesis mixture was transferred to a 100 °C oven for a period of heating between 0–7 days depending on zeolite type (Supplementary Fig. 2), where 3 days was the nominal time. The solid product was then recovered as follows. Synthesis mixtures were washed with DI water (30 g) and transferred to a centrifuge tube using a nickel spatula. After centrifugation (5 min, 13,000 rpm), the supernatant solution was decanted. This procedure was repeated twice more with ~40 g DI water. The gel product was dried overnight in an incubator (~60 °C).

Zeolite syntheses designed to simulate glasses

Growth mixtures were prepared with molar compositions 60.2 SiO_2:*a* Al_2O_3:*b* CaO:*c* ZrO_2:*d* B_2O_3:*e* SnO_2:30.1 Na_2O:1270 H_2O where *a, b, c, d,* and *e* are selected to achieve the glass compositions displayed in Supplementary Table 2. The same approach for conventional zeolite synthesis was used for zeolite synthesis designed to simulate glasses with a few procedural changes. Sodium hydroxide and sodium aluminate were dissolved first like in conventional synthesis, followed individually by boric acid, tin (IV) chloride pentahydrate, zirconium (IV) oxide, calcium hydroxide, and finally LUDOX AS-40 which immediately causes the mixture to coagulate. The same procedure described above was performed on the resulting gel, and the resulting solid product was recovered in the same manner described above for conventional zeolite synthesis.

Materials characterization

Powder X-ray diffraction (PXRD) patterns were collected on a Rigaku diffractometer using Cu Kα radiation (40 kV, 40 mA). Data were collected with a step size of 0.02 (2θ) at a rate of 8.33 steps per second. Phase quantification was performed using the fundamental parameters approach using TOPAS software[2]. Magnesium oxide was mixed into each zeolite sample as an internal standard at ~10 wt% to normalize PXRD patterns and determine the crystalline and amorphous fraction of each sample.

DATA AVAILABILITY

The data that support the findings of this study are available from the corresponding authors upon reasonable request.

Received: 28 September 2022; Accepted: 20 November 2022;
Published online: 12 January 2023

REFERENCES

1. Gin, S. et al. An international initiative on long-term behavior of high-level nuclear waste glass. *Mater. Today* **16**, 243–248 (2013).
2. Vienna, J. D., Ryan, J. V., Gin, S. & Inagaki, Y. Current understanding and remaining challenges in modeling long-term degradation of borosilicate nuclear waste glasses. *Int. J. Appl. Glass Sci.* **4**, 283–294 (2013).
3. Ojovan, M. I. On alteration rate renewal stage of nuclear waste glass corrosion. *MRS Adv.* **5**, 111–120 (2020).
4. Van Iseghem, P. & Grambow, B. The long-term corrosion and modelling of two simulated Belgian reference high-level waste glasses. *MRS Proc.* **112**, 631–639 (1987).
5. Strachan, D. M. & Croak, T. L. Compositional effects on long-term dissolution of borosilicate glass. *J. Non-Cryst. Solids* **272**, 22–33 (2000).
6. Strachan, D. M. & Neeway, J. J. Effects of alteration product precipitation on glass dissolution. *Appl. Geochem.* **45**, 144–157 (2014).
7. Fournier, M., Gin, S. & Frugier, P. Resumption of nuclear glass alteration: state of the art. *J. Nucl. Mater.* **448**, 348–363 (2014).
8. Neeway, J. J. et al. Acceleration of glass alteration rates induced by zeolite seeds at controlled pH. *Appl. Geochem.* **113**, 104515 (2020).
9. Maldonado, M., Oleksiak, M. D., Chinta, S. & Rimer, J. D. Controlling crystal polymorphism in organic-free synthesis of Na-zeolites. *J. Am. Chem. Soc.* **135**, 2641–2652 (2013).
10. Lobo, R. F., Zones, S. I. & Davis, M. E. Structure-direction in zeolite synthesis. *J. Incl. Phenom.* **21**, 47–78 (1995).
11. Asselman, K. et al. Super-ions of sodium cations with hydrated hydroxide anions: inorganic structure-directing agents in zeolite synthesis. *Mater. Horiz.* **8**, 2576–2583 (2021).
12. Shin, J., Jo, D. & Hong, S. B. Rediscovery of the importance of inorganic synthesis parameters in the search for new zeolites. *Acc. Chem. Res.* **52**, 1419–1427 (2019).
13. Jain, R., Mallette, A. J. & Rimer, J. D. Controlling nucleation pathways in zeolite crystallization: seeding conceptual methodologies for advanced materials design. *J. Am. Chem. Soc.* **143**, 21446–21460 (2021).
14. Mallette, A. J. et al. Heteroatom manipulation of zeolite crystallization: stabilizing Zn-FAU against interzeolite transformation. *JACS Au* **2**, 2295–2306 (2022).

15. Chawla, A. et al. Crystallization of potassium-zeolites in organic-free media. *Micropor. Mesoporous Mater.* **341**, 1–14 (2022).
16. Van Tendeloo, L., Gobechiya, E., Breynaert, E., Martens, J. A. & Kirschhock, C. E. A. Alkaline cations directing the transformation of FAU zeolites into five different framework types. *Chem. Comm.* **49**, 11737–11739 (2013).
17. Pabalan, R. T. & Bertetti, F. P. Cation-exchange properties of natural zeolites. *Rev. Miner. Geochem.* **45**, 453–518 (2001).
18. Khodabandeh, S. & Davis, M. E. Zeolites P1 and L as precursors for the preparation of alkaline-earth zeolites. *Micropor. Mater.* **12**, 347–359 (1997).
19. Xu, B., Smith, P. & Wingate, C. & De Silva, L. The effect of calcium and temperature on the transformation of sodalite to cancrinite in Bayer digestion. *Hydrometallurgy* **105**, 75–81 (2010).
20. Lee, Y.-J., Lee, J. S. & Yoon, K. B. Synthesis of long zeolite-L crystals with flat facets. *Micropor. Mesoporous Mater.* **80**, 237–246 (2005).
21. Liang, Y., Jacobson, A. J. & Rimer, J. D. Strontium ions function as both an accelerant and structure-directing agent of chabazite crystallization. *ACS Mater. Lett.* **3**, 187–192 (2020).
22. Cocks, P. A. & Pope, C. G. Salt effects on the synthesis of some aluminous zeolites. *Zeolites* **15**, 701–707 (1995).
23. Zones, S. I. et al. The fluoride-based route to all-silica molecular sieves; a strategy for synthesis of new materials based upon close-packing of guest–host products. *C. R. Chim.* **8**, 267–282 (2005).
24. Zones, S. I., Darton, R. J., Morris, R. & Hwang, S.-J. Studies on the role of fluoride ion vs reaction concentration in zeolite synthesis. *J. Phys. Chem. B* **109**, 652–661 (2005).
25. Vattipalli, V., Paracha, A. M., Hu, W., Chen, H. & Fan, W. Broadening the scope for fluoride-free synthesis of siliceous zeolites. *Angew. Chem., Int. Ed. Engl.* **57**, 3607–3611 (2018).
26. Guth, J. L. et al. *Zeolite Synthesis in the Presence of Fluoride Ions, in Zeolite Synthesis* (ACS Publications, 1989).
27. Jon, H., Lu, B., Oumi, Y., Itabashi, K. & Sano, T. Synthesis and thermal stability of beta zeolite using ammonium fluoride. *Micropor. Mesoporous Mater.* **89**, 88–95 (2006).
28. Camblor, M. A., Corma, A. & Valencia, S. Synthesis in fluoride media and characterisation of aluminosilicate zeolite beta. *J. Mater. Chem.* **8**, 2137–2145 (1998).
29. Eilertsen, E. A., Arstad, B., Svelle, S. & Lillerud, K. P. Single parameter synthesis of high silica CHA zeolites from fluoride media. *Micropor. Mesoporous Mater.* **153**, 94–99 (2012).
30. Tolborg, S. et al. Incorporation of tin affects crystallization, morphology, and crystal composition of Sn-Beta. *J. Mater. Chem. A* **2**, 20252–20262 (2014).
31. Opanasenko, M. et al. Synthesis and post-synthesis transformation of germanosilicate zeolites. *Angew. Chem. Int. Ed. Engl.* **59**, 19380–19389 (2020).
32. Crum, J. V. et al. Seeded Stage III glass dissolution behavior of a statistically designed glass matrix. *J. Am. Ceram. Soc.* **104**, 4145–4162 (2021).
33. Russell, R. L. et al. Enhanced Hanford Low-Activity Waste Glass Property Data Development: Phase 2 PNNL-28838 Rev 2 Pacific Northwest National Laboratory (PNNL), Richland, WA (United States) (2021).
34. Parruzot, B. et al. Effect of zeolite type, temperature, and pH on Stage III glass alteration behavior for two nuclear waste glasses *J. Nucl. Mater.* **567**, 1–14 (2022).
35. Oleksiak, M. D. et al. Synthesis strategies for ultrastable zeolite GIS polymorphs as sorbents for selective separations. *Eur. J. Chem.* **22**, 16078–16088 (2016).
36. Fournier, M., Gin, S., Frugier, P. & Mercado-Depierre, S. Contribution of zeolite-seeded experiments to the understanding of resumption of glass alteration. *npj Mater. Degrad.* **1**, 1–13 (2017).
37. Conato, M. T., Oleksiak, M. D., McGrail, B. P., Motkuri, R. K. & Rimer, J. D. Framework stabilization of Si-rich LTA zeolite prepared in organic-free media. *Chem. Comm.* **51**, 269–272 (2015).
38. Sharma, P., Song, J.-S., Han, M. H. & Cho, C.-H. GIS-NaP1 zeolite microspheres as potential water adsorption material: Influence of initial silica concentration on adsorptive and physical/topological properties. *Sci. Rep.* **6**, 1–26 (2016).
39. Fan, W., Shirato, S., Gao, F., Ogura, M. & Okubo, T. Phase selection of FAU and LTA zeolites by controlling synthesis parameters. *Micropor. Mesoporous Mater.* **89**, 227–234 (2006).
40. Zhu, G. et al. Synthesis and characterization of high-quality zeolite LTA and FAU single nanocrystals. *Chem. Mater.* **10**, 1483–1486 (1998).
41. Oleksiak, M. D., Soltis, J. A., Conato, M. T., Penn, R. L. & Rimer, J. D. Nucleation of FAU and LTA zeolites from heterogeneous aluminosilicate precursors. *Chem. Mater.* **28**, 4906–4916 (2016).
42. Freeman, E. E., Neeway, J. J., Motkuri, R. K., Rimer, J. D. & Mpourmpakis, G. Understanding initial zeolite oligomerization steps with first principles calculations. *AlChE J.* **66**, e17107 (2020).
43. Sonnet, P. M. Burtite, calcium hexahydroxostannate, a new mineral from El Hamman, central Morocco. *Canad. Miner.* **19**, 397–401 (1981).
44. Lew, C. M., Rajabbeigi, N. & Tsapatsis, M. Tin-containing zeolite for the isomerization of cellulosic sugars. *Micropor. Mesoporous Mater.* **153**, 55–58 (2012).
45. Kasula, M., Spanos, A. P., Ford, L. & Brunelli, N. A. Investigating the impact of synthesis conditions to increase the yield and tin incorporation efficiency for Lewis acid nano-Sn-MFI zeolites. *Ind. Eng. Chem. Res.* **61**, 1977–1984 (2022).
46. Kinrade, S. D., Syvitski, R. T., Marat, K. & Knight, C. T. G. Two-dimensional silicon-29/Tin-117 NMR evidence of aqueous stannosilicate anions. *J. Am. Chem. Soc.* **118**, 4196–4197 (1996).
47. Parruzot, B. et al. Multi-glass investigation of Stage III glass dissolution behavior from 22 to 90 °C triggered by the addition of zeolite phases. *J. Nucl. Mater.* **523**, 490–501 (2019).
48. Gin, S. et al. The fate of silicon during glass corrosion under alkaline conditions: a mechanistic and kinetic study with the International Simple Glass. *Geochim. Cosmochim. Acta* **151**, 68–85 (2015).
49. Malkovsky, V. I., Yudintsev, S. V., Ojovan, M. I. & Petrov, V. A. The influence of radiation on confinement properties of nuclear waste glasses. *Sci. Technol. Nucl.* **2020**, 8875723 (2020).
50. Chen, X. et al. Gamma-ray irradiation to accelerate crystallization of mesoporous zeolites. *Angew. Chem.* **132**, 11421–11425 (2020).

ACKNOWLEDGEMENTS

This work was supported by the U.S. Department of Energy (DOE), Nuclear Energy University Program (DOE-NEUP) under grant number 18-15496. J.D.R. received additional support from The Welch Foundation (grant number E-1794). Pacific Northwest National Laboratory (PNNL) is operated by Battelle Memorial Institute for the DOE under contract DE-AC05-76RL01830. We thank Xiaonan Lu and Jarrod Crum of PNNL for their helpful review of the paper.

AUTHOR CONTRIBUTIONS

The project was conceived by J.D.R., J.J.N., R.K.M., and G.M. All zeolite crystallization experiments were performed by A.J.M. and J.D.R. Zeolite characterization and data analysis were performed by A.J.M., J.T.R., and J.J.N. The original draft of the manuscript was prepared by A.J.M. and J.D.R., with feedback from J.T.R., J.J.N., R.K.M., and G.M. All authors contributed to editing and finalizing the manuscript.

COMPETING INTERESTS

The authors declare no competing interests.

ADDITIONAL INFORMATION

Supplementary information The online version contains supplementary material available at https://doi.org/10.1038/s41529-022-00310-9.

Correspondence and requests for materials should be addressed to James J. Neeway or Jeffrey D. Rimer.